Progress In Electromagnetics Research, Vol. 105, 1–13, 2010

3D SLICED TOMOGRAPHIC INVERSE SCATTERING EXPERIMENTAL RESULTS

R. Solimene, A. Brancaccio, R. Di Napoli, and R. Pierri

Dipartimento di Ingegneria dell'Informazione
via Roma 29, I-81031 Aversa, Italy

Abstract—The problem of imaging three-dimensional strong scatterers by means of a two-dimensional sliced tomographic reconstruction algorithm is dealt with. In particular, the focus of the paper is on the experimental validation of the involved inversion algorithm thanks to measurements collected in a controlled environment. A simple strategy exploiting reconstructions obtained at different time instants in order to detect slowly moving scatterers is also experimentally validated.

1. INTRODUCTION

Microwave imaging is a research field which finds application in many contexts such as radar and ground penetrating radar imaging [1], non-destructive testing or evaluation of materials [2], medical imaging [3], just to mention a few examples.

From a mathematical point of view the problem consists of inverting the scattering equations for an object function which describes the scatterers in terms of their dielectric and conductivity properties and/or their spatial supports or shapes. In any case, it is well known that the problem is nonlinear and ill-posed [4].

Many inversion methods are widespread in the literature that tackle the problem trying to dominate the nonlinearity. They results in iterative optimization inversion schemes which suffer from the false solutions [5] and generally require a high computational cost. Also stochastic optimization methods [6] are still time consuming when the number of unknowns is high.

Inversion schemes based on approximated linear models allow to drastically simplify the problem and to overcome the drawbacks mentioned above but they work for a very limited class of scatterers [7].

Corresponding author: A. Brancaccio (adriana.brancaccio@unina2.it).

However, in many applications, the primary concern is to detect and localize the scatterers. Within this framework, linear inversion schemes are worth adopting as it has been shown that they work well beyond the limits of the linear model upon which they are based [8].

In this contribution, we consider the case of strong scatterers. Accordingly, the *linear distributional approach* founded on the Kirchhoff approximation is adopted [8, 9]. However, even under linear models dealing with three-dimensional (3D) geometry could require a high computational cost. Therefore, here we exploit a slice method where the scene is retrieved as an interpolation of two-dimensional (2D) reconstructions.

It is well known that, as diffraction and scattering phenomena at microwave frequencies are relevant, the sliced approach does not permit to obtain quantitative reconstructions [10, 11]. However, it has been also shown, by numerical examples, that it allows to localize and to roughly retrieve the silhouette of elongated scatterers [12]. But this is just the aim pointed out before. In particular, here we want to find a further confirmation of the approach validity by employing experimental data.

To this end, measurements are collected in a free-space controlled environment at the Electromagnetic Diagnostics Laboratory of the Second University of Naples.

Note that preliminary experimental results have been already obtained in [13, 14]. However, they are concerned with two-dimensional (single-slice) reconstructions.

A reflection-mode multi-bistatic/multifrequency configuration is exploited and an anthropomorphic mannequin covered by aluminium foils is used as a scatterer. Moreover, the possibility of taking measurements over a limited set of spatial points is considered. This is of particular interest because it affects time required to collect data, particularly when scanning is achieved through a moving system, and also impacts on the system complexity when a measurement array is employed.

Finally, a simple procedure to track slowly moving scatterers, presented in [15], based on the incoherent difference between two different images of the same scene retrieved at different times, is also validated for the 3D case.

The plan of the paper is the following. In Section 2, we describe the geometry of the problem and briefly recall the inversion scheme. In Section 3, we present the measurement set up and in Section 4 the experimental reconstructions. Conclusions end the paper.

2. MATHEMATICAL FORMULATION AND INVERSION ALGORITHM

A pictorial view of the experimental set up, where three-dimensional scatterers are embedded in free-space whose dielectric permittivity and magnetic permeability are denoted as ϵ_0 and μ_0, respectively, is shown in Fig. 1.

Scatterers are illuminated by an y-polarized source whose position $\underline{r}_S = (x_S, y_S, 0)$ changes within a planar measurement aperture $\Sigma = [X_{M\,\min}, X_{M\,\max}] \times [Y_{M\,\min}, Y_{M\,\max}]$ at $z = 0$. The source radiates in the frequency band $\omega \in [\omega_{\min}, \omega_{\max}]$ and the scattered field is collected at positions standing at a fixed offset from the source, $\underline{r}_O = (x_S + \Delta x, y_S, 0)$, while the source moves.

For imaging purposes, we assume that the scatterers reside within an a priori known spatial region $D = [X_{I\,\min}, X_{I\,\max}] \times [Y_{I\,\min}, Y_{I\,\max}] \times [Z_{I\,\min}, Z_{I\,\max}]$, addressed as investigation domain.

Starting from scattered field measurements the 3D inverse scattering problem is tackled by a 2D sliced inversion algorithm. That is, the scattered field collected over each observation line at different heights (i.e., at different y-coordinates) of the observation domain Σ is exploited to obtain a 2D slice (i.e., in the x-z plane) of the investigated scene in correspondence to the same height. More in detail, we assume to collect only the y-component of the scattered field and the slice reconstruction is treated as a two-dimensional and scalar inverse problem. Hence, the 3D reconstruction is obtained by solving a collection of 2D problems at different heights $y_i \in (y_1, \ldots, y_M)$. Moreover, as we are interested in highly contrasted objects (i.e., objects whose electromagnetic features are very different from those of the

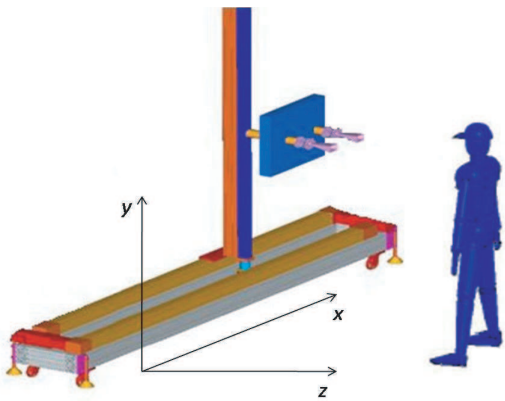

Figure 1. Experimental set up pictorial view.

free-space), we assume the limit-case of perfect electric conductors to schematize them. Accordingly, the Kirchhoff approximation is employed to linearize the inverse problem [9].

By assuming that the objects are some wavelengths far from the measurement line (so that the asymptotic expression for the Green's functions applies [16]), the problem of reconstructing the 2D slices amounts to solving the following integral equation

$$E_s^{(m)}(x_O, x_S; \omega) = -\frac{j\omega\mu_0}{4\pi} \int_{\Gamma_{ill}(y_m)} \frac{\exp\{-jk\left[R_O(\ell) + R_S(\ell)\right]\}}{\sqrt{R_O(\ell) R_S(\ell)}} \times \left[\hat{n}(\ell) \cdot \hat{r}(\ell)\right] d\ell, \tag{1}$$

where $E_s^{(m)}$ indicates the scattered field at the height y_m, $k = \omega\sqrt{\varepsilon_0\mu_0}$ is the wavenumber of the host medium, ℓ is the curvilinear abscissa on the scatterer's contour $\Gamma(y_m)$, R_S (R_O) is the distance between the source (the receiving) point from the generic point $[x(\ell), y_m, z(\ell)] \in \Gamma_{ill}(y_m)$, $\Gamma_{ill}(y_m)$ is the illuminated side of the object's contour (at the height y_m), $\hat{n}$ is the outward directed normal to the scatterers' contours and $\hat{r}$ is the unitary vector indicating the direction from the source point towards the current contour's point.

It is worth remarking that, in Eq. (1), we considered a two-dimensional dipole as source [17]. Therefore, in the following experiments the actual antennas plane-wave spectrum is not accounted for.

We note that both the scalar product $\hat{n} \cdot \hat{r}$ and Γ_{ill} depend on the source position. However, by invoking stationary phase arguments, and if the offset Δx between the source and the observation is small with respect to R_O and R_S, then the point of $\Gamma_{ill}(y_m)$ that gives significant contribution to the integral in (1) is the geometrical optics (GO) reflection point. Accordingly, $\hat{n} \cdot \hat{r} \simeq -1$. Moreover, we can extend the integral to the union of the different $\Gamma_{ill}(y_m)$ (corresponding to different x_S), let us call it $\tilde{\Gamma}(y_m)$. This way, neither the unknown nor the mathematical relationship linking the unknown to the scattered field depend on the source position [17] and the problem can now be stated as the inversion of the following linear integral operator

$$E_s^{(m)}(x_O, x_S; \omega) = \frac{j\omega\mu_0}{4\pi} \int_{D_T} \frac{\exp\left[-jk\left(R_O + R_S\right)\right]}{\sqrt{R_O R_S}} \times \delta_{\tilde{\Gamma}(y_m)}(x, z) dx dz, \tag{2}$$

where the actual unknown of the problem is the single-layer distribution $\delta_{\tilde{\Gamma}(y_m)}(x, z)$ just supported over the curve $\tilde{\Gamma}(y_m)$ and D_T is the investigation domain cross section in the x-z plane, that is $D_T = [X_{I\,\min}, X_{I\,\max}] \times [Z_{I\,\min}, Z_{I\,\max}]$.

The inversion of Eq. (2) is achieved first by means of a truncated singular values decomposition (TSVD) schemes [18], that is

$$\mathcal{R}\delta_{\tilde{\Gamma}(y_m)} = \sum_{n=1}^{N_T} \frac{< E_s^{(m)}, v_n >}{\sigma_n} u_n, \tag{3}$$

where $\{u_n, v_n, \sigma_n\}_{n=1}^{\infty}$ is the singular system of (2), N_T is the truncation index and $\mathcal{R}\delta_{\tilde{\Gamma}(y_m)}$ is the regularized reconstruction. Then a thresholding procedure is exploited to curtail spurious artifacts and noise nonsense as described in [12]. Note that the singular system can be calculated once, because it does not depend on the height y_m.

Once the two-dimensional slice reconstructions have been obtained, the three-dimensional representation of the scatterer is obtained by superimposing the two-dimensional reconstructions

$$\mathcal{R}\delta_{\tilde{\Gamma}}(x, y, z) = \begin{pmatrix} \mathcal{R}\delta_{\tilde{\Gamma}(y_1)}(x, z) \\ \cdots \\ \mathcal{R}\delta_{\tilde{\Gamma}(y_M)}(x, z) \end{pmatrix}. \tag{4}$$

Finally, an interpolation along y follows [12].

3. MEASUREMENT SYSTEM

The measurement set-up consists of a positioning system and of a vectorial network analyzer (VNA) which are remotely controlled and synchronized by a PC thanks to a customized LabView software.

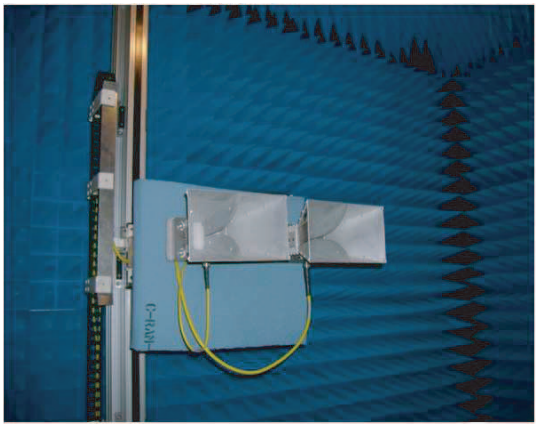

Figure 2. Picture of the planar scanner placed in the anechoic chamber.

The positioning system is placed into a shielded anechoic chamber (with internal dimensions of 2.4 m in depth, 3.4 m in length and 2.6 m in height) and is made of two vertical towers which can move independently over a horizontal linear positioner. As a multi-bistatic configuration is of concern, here only a single vertical tower, where two antennas are mounted at a fixed offset between each other, is used (see Fig. 2). The antennas are two wide band ridged horns (Schwarzbeck Mess-Elektronik), suitably aligned so that they scan the same plane (see Fig. 2), working in the 0.8–5.2 GHz band.

The VNA is an Anritsu model MS4624D working in the band [10 MHz–9 GHz]. The measured parameter is the transmission coefficient S_{21} between the ports 1 and 2 of the VNA.

In order to make measurements suitable for the inversion algorithm, first a standard "frequency transmission response" calibration is performed at the end of the cable chain, that is at the antenna input sections. Then, as the inversion algorithm exploits the scattered field measurements, free-space measurements are needed so that the scattered field is obtained by difference. This also allows to mitigate the direct coupling between the antennas as long as it remains the same over the two measurements.

4. RECONSTRUCTION RESULTS

This section is devoted to showing some reconstructions based on experimentally collected data in order to assess the reconstruction capabilities of the inversion algorithm.

The experimental data are collected in the frequency band [0.8, 3.2] GHz by employing a measurement aperture $\Sigma = [35, 235]\,\text{cm} \times [60, 200]\,\text{cm}$, with the transmitting and the receiving antennas separated by an offset $\Delta x = 30\,\text{cm}$ (measured between the two aperture centers). The investigation domain is $D = [35, 235]\,\text{cm} \times [60, 200]\,\text{cm} \times [100, 170]\,\text{cm}$ (the quota along z is measured starting from the antenna aperture). A plastic mannequin 180 cm in height covered by aluminium foils is considered as the scatterer. The mannequin has been placed over a dielectric pedestal 10 cm in height so that it covers the investigation domain from $y = 60\,\text{cm}$ to $y = 190\,\text{cm}$ (see Fig. 3).

The following 3D reconstructions are given in terms of isosurface representations and report the modulus of the regularized retrieved unknown, $|\mathcal{R}\delta_{\tilde{\Gamma}}|$, which in turn is obtained by retaining in the TSVD expansion the singular functions corresponding to the singular values not below $-20\,\text{dB}$ (this truncation roughly corresponds to the beginning of abrupt decay of the singular values). A picture of the mannequin is superimposed to each reconstruction for comparison purposes.

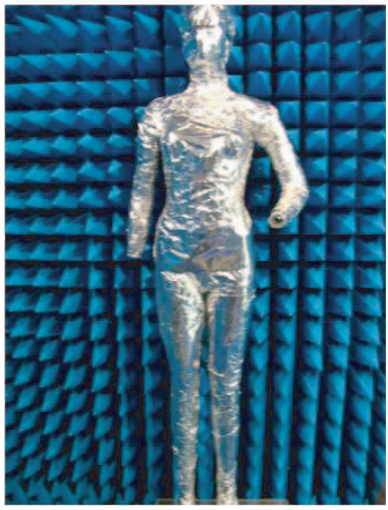

Figure 3. Picture of the mannequin within the anechoic chamber.

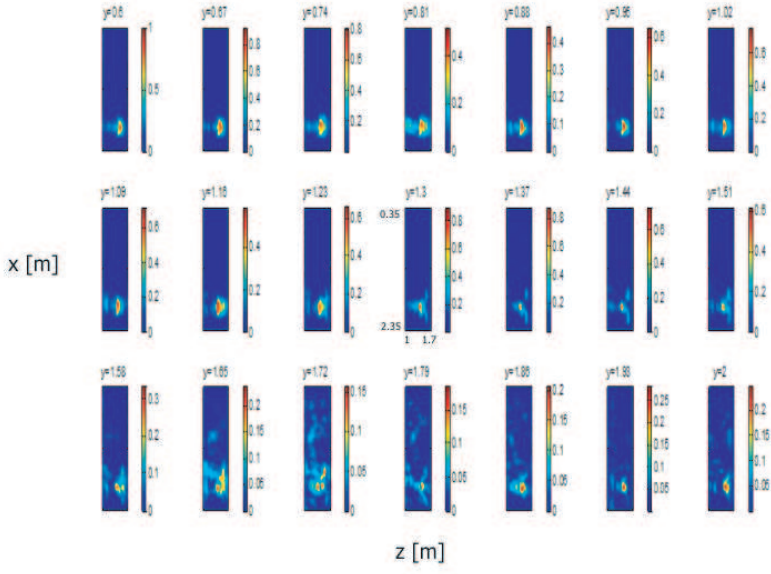

Figure 4. Slice reconstructions of the mannequin: 11 uniformly spaced frequencies and 51 measurements points along the x-axis have been used.

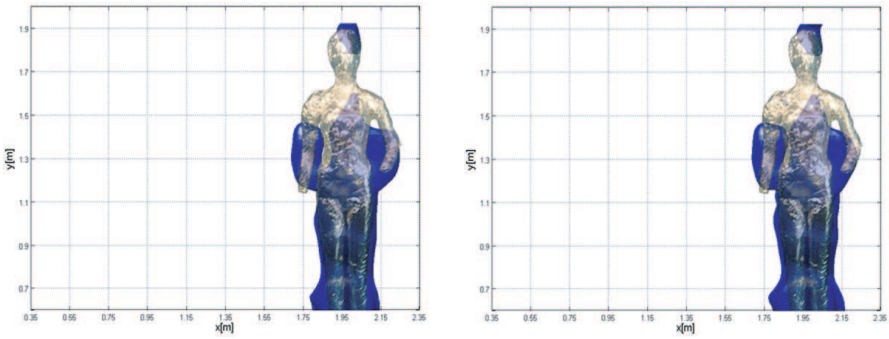

Figure 5. Frontal view of the 3D reconstruction (blue) along with the mannequin picture (grey) at its actual position and dimension. Reconstruction obtained by sampling each measurement line with 51 (left panel) and 26 (right panel) points.

The first experimental result is shown in Fig. 4 and in the left panel of Fig. 5. It refers to the case where the mannequin center is roughly located at $x = 195\,\text{cm}$ and $z = 145\,\text{cm}$. For such a case, 21 equally spaced slices have been considered and for each slice the measurement line has been uniformly sampled at a step of 4 cm, so that 51 measurements have been taken. Moreover, 11 uniformly spaced frequencies, within the band reported above, have been used. Fig. 4 shows the different slice reconstructions from which it can be appreciated that the scatterer is detected and correctly localized. After obtaining the 2D slices, each of them is first normalized to the "global" maximum (i.e., the maximum over all the slices) and then thresholded as described in [19]. In the left panel of Fig. 5 the corresponding 3D (frontal view) isosurface representation is reported. As can be seen, the phantom is not only very well localized but also its silhouette is retrieved.

A critical point towards a fast imaging process (i.e., data acquisition plus image formation) is the number of data to be used which affects data and process time as well as the needed memory storage.

To cope with this question the evaluation of the so-called number of degrees of freedom (NDF) plays a central role [20].

Therefore, in order to make the imaging computationally more effective results concerning the NDF reported in [21] have been adopted. In particular, for the measurement configuration exploited above, it was found that at the highest adopted frequency 26 measurement points (for each slice) are enough (this number has been also maintained for the lower frequencies). As to the frequencies,

we still adopt 11 frequencies, which are slightly beyond the optimal number derived in [22], because time required for frequency sweeping is negligible with respect to spatial scanning. The reconstruction of the same scatterer by employing the new measurement parameters is reported in the right panel of Fig. 5. As can be seen, the quality of the reconstruction is practically the same as the previous case. This is also a remarkable result if one looks at other imaging methods present in the literature which have shown to work for a finer data collection grid [23, 24].

In view of the reduced number of data the imaging algorithm takes few seconds to achieve the images. Instead, the time needed to acquire the data is still a critical figure for sliding systems as the one at hand. However, if the measurements were taken quasi-instantaneously, for example by employing an antenna array, changes of the scene during data acquirement could be neglected (so avoiding image focusing degradation). In this case, a simple procedure able to counteract the clutter due to static scatterers could be employed. For example, a procedure based on the incoherent difference between two reconstructions obtained at two different instants of time in principle allows to discern a moving target from static objects [15].

In order to verify experimentally the principle of the method proposed in [15], we turn to consider two different situations where a static scatter is present in the scene whereas the mannequin is located at two different positions. The static scatterer is a metallic coat hanger 1.7 m in height whose main part is a 5 cm diameter cylinder 1.5 m

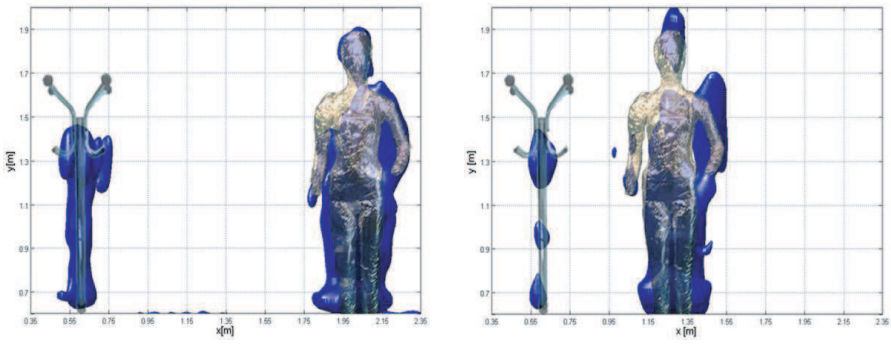

Figure 6. Frontal view of 3D reconstructions (blue) for two different scatterers, the mannequin and a coat hanger, whose pictures are shown in grey at their actual positions and dimensions. The panel on the left is referred as the case 1 and the panel on the right as the case 2, where the two scatterers are closer each to the other. Reconstructions obtained by sampling each measurement line with 26 points.

in height. The reconstructions corresponding to these two cases are reported in Fig. 6: in both the images all the objects in the scene are well localized even though in the second case the scatterer on the left is reconstructed worse than in the first case. This is because the mannequin is more strongly (in amplitude) reconstructed when it is located in the middle of the scene. Therefore, while applying the threshold (which is set up according to the maximum of the overall reconstruction) some parts of the reconstruction of the scatterer on the left are discarded as well.

The presence of a moving scatterer can be evidenced by representing the positive values of the pixel by pixel difference between reconstructions related to data taken at different instants of time. As an example, let us consider the two scenes reported in Fig. 6, indicated as 1 (left) and 2 (right) respectively, as a time sequence where the mannequin plays the role of the "moving" scatterer. In order to localize it, we represent the quantities

$$\Delta\delta_{\tilde{\Gamma}2} = \begin{cases} |\mathcal{R}\delta_{\tilde{\Gamma}}|_2 - |\mathcal{R}\delta_{\tilde{\Gamma}}|_1 & \text{if} \quad |\mathcal{R}\delta_{\tilde{\Gamma}}|_2 - |\mathcal{R}\delta_{\tilde{\Gamma}}|_1 > 0 \\ 0 & \text{if} \quad |\mathcal{R}\delta_{\tilde{\Gamma}}|_2 - |\mathcal{R}\delta_{\tilde{\Gamma}}|_1 < 0 \end{cases} \tag{5}$$

and

$$\Delta\delta_{\tilde{\Gamma}1} = \begin{cases} |\mathcal{R}\delta_{\tilde{\Gamma}}|_1 - |\mathcal{R}\delta_{\tilde{\Gamma}}|_2 & \text{if} \quad |\mathcal{R}\delta_{\tilde{\Gamma}}|_1 - |\mathcal{R}\delta_{\tilde{\Gamma}}|_2 > 0 \\ 0 & \text{if} \quad |\mathcal{R}\delta_{\tilde{\Gamma}}|_1 - |\mathcal{R}\delta_{\tilde{\Gamma}}|_2 < 0 \end{cases} \tag{6}$$

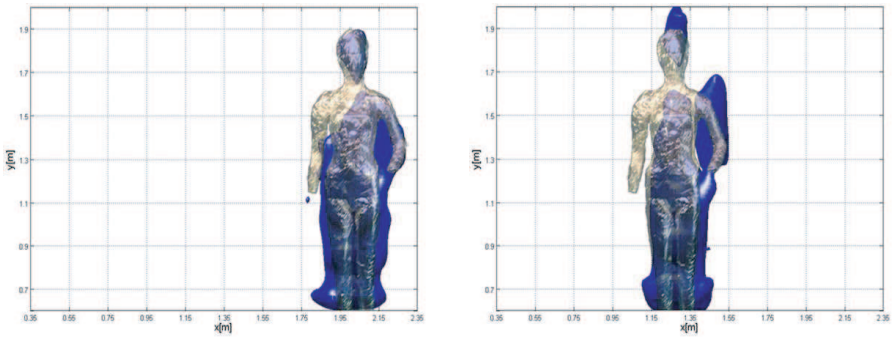

Figure 7. "Difference" 3D reconstructions (blue) and picture of the "moving" mannequin (grey). The panel on the left reports $\triangle\delta_{\tilde{\Gamma}1}$ (the mannequin "moved" from the left to the right) whereas the panel on the right reports $\triangle\delta_{\tilde{\Gamma}2}$ (the mannequin "moved" from the right to the left). Reconstructions obtained by sampling each measurement line with 26 points.

where $|\mathcal{R}\delta_{\tilde{\Gamma}}|_1$ and $|\mathcal{R}\delta_{\tilde{\Gamma}}|_2$ are the reconstruction reported in the left and right panel of Fig. 6, respectively, and $\Delta\delta_{\tilde{\Gamma}1}$ ($\Delta\delta_{\tilde{\Gamma}2}$) is the difference image actually employed to localized the moving scatterer when the time-sequence is scene 2-scene 1 (scene 1-scene 2). The result of this procedure is reported in Fig. 7. As can be seen, the procedure works very well and the results are quite remarkable if one thinks that it does not require a reference background image as is the case of other difference image procedures [25].

5. CONCLUSIONS

We have checked experimentally the linear slice based inversion scheme for reconstructing 3D strong scattering objects resembling in shape the human body. The experiments have been conducted for a free-space situation within a controlled environment. However, the measurement parameters have been chosen with TWI applications in mind (i.e., choice of the frequency band, reflection mode set-up). Therefore, this contribution can be meant as preliminary to such a kind of applications. Despite the simplicity of the inversion algorithm, the analysis has shown that it allows to localize and to roughly determine the shape of the scatterers dealing with large (in terms of the wavelength) investigation domains. Moreover, by selecting the measurement points and the frequencies according to the degrees of freedom of the scattered field, the reconstruction algorithm becomes very quickly. This opens the way to the possibility of detecting moving targets in order to discern a human being from static background clutter. In this regard, a simple procedure based on the incoherent difference between two reconstructions (not requiring a reference background image) to detect changes in the imaging scenario has been presented and validated. Of course, the results presented herein have to be meant as a proof of the principle. Indeed, we have used a sliding system to synthesize the measurement aperture which requires a non negligible time to acquire the data, even though data are collected according to the NDF. Antenna arrays would be a more suitable choice to make the change detection technique useful for practical real time moving target tracking.

REFERENCES

1. Daniels, D. J., *Ground Penetrating Radar*, 2nd edition, IEE Radar, Sonar and Navigation Series 15, UK, 2004.
2. Marklein, R., K. J. Langenberg, K. Mayer, J. Miao, A. Shlivinski, A. Zimmer, W. Miller, V. Schmitz, C. Kohl, and U. Mletzko,

"Recent applications and advances of numerical modeling and wavefield inversion in nondestructive testing," *Adv. in Radio Sci.*, Vol. 3, 167–174, 2005.

3. Yu, C., M. Yuan, J. Stang, E. Bresslour, R. T. George, A. Ybarra, W. T. Joines, and Q. H. Liu, "Active microwave imaging II: 3-D system prototype and image reconstruction from experimental data," *IEEE Trans. Microw. Theor. Tech.*, Vol. 56, No. 4, 991–1000, 2008.
4. Chew, W. C., *Waves and Fields in Inhomogeneous Media*, IEEE Press, Piscataway, NJ, 1995.
5. Fhager, A. and M. Persson, "Using a priori data to improve the reconstruction of small objets in microwave tomography," *IEEE Trans. Microw. Theor. Tech.*, Vol. 55, No. 11, 2454–2462, 2007.
6. Pastorino, M., "Stochastic optimization methods applied to microwave imaging: A review," *IEEE Trans. Ant. Prop.*, Vol. 55, No. 3, 538–548, 2007.
7. Slaney, M., A. C. Kak, and L. E. Larsen, "Limitation of imaging with firt-order diffraction tomography," *IEEE Trans. Microw. Theor. Tech.*, Vol. 32, No. 8, 860–874, 1984.
8. Pierri, R., A. Liseno, R. Solimene, and F. Soldovieri, "Beyond physical optics SVD shape reconstruction of metallic cylinders," *IEEE Trans. Ant. Propag.*, Vol. 54, No. 2, 655–665, 2006.
9. Bojarski, N. N., "A survey of the physical optics inverse scattering identity," *IEEE Trans. Ant. Prop.*, Vol. 30, No. 5, 980–989, 1982.
10. Zhang, Z. Q. and Q. H. Liu, "Three-dimensional nonlinear image reconstruction for microwave biomedical imaging," *IEEE Transactions on Biomedical Engineering*, Vol. 51, 544–548, 2004.
11. Semenov, S. Y., R. H. Svenson, A. E. Boulyshev, A. E. Souvorov, V. Y. Borisov, Y. Sizov, A. N. Starostin, K. R. Dezern, G. T. Tatsis, and V. Y. Baranov, "Microwave tomography: Two-dimensional system for biological imaging," *IEEE Transactions on Biomedical Engineering*, Vol. 43, 869–876, 1996.
12. Solimene, R., F. Soldovieri, G. Prisco, and R. Pierri, "Three-dimensional microwave tomography by a 2-D slice-based reconstruction algorithm," *IEEE Geosc. Rem. Sens. Lett.*, Vol. 4, No. 4, 556–560, 2007.
13. Soldovieri, F. and R. Solimene, "Through-wall imaging via a linear inverse scattering algorithm," *IEEE Geosc. Rem. Sens. Lett.*, Vol. 4, No. 4, 513–517, 2007.
14. Solimene, R., A. Brancaccio, R. Pierri, and F. Soldovieri, "TWI experimental results by a linear inverse scattering approach,"

Progress In Electromagnetics Research, Vol. 91, 259–272, 2009.

15. Soldovieri, F., R. Solimene, and R. Pierri, "A simple strategy to detect changes in through the wall imaging," *Progress In Electromagnetics Research M*, Vol. 7, 1–13, 2009.
16. Felsen, L. B. and N. Marcuwitz, *Radiation and Scattering of Waves*, Prentice-Hall, Englewood Cliffs, NJ, 1973.
17. Soldovieri, F., A. Brancaccio, G. Prisco, G. Leone, and R. Pierri, "A kirchhoff-based shape reconstruction algorithm for the multimonostatic configuration: The realistic case of buried pipes," *IEEE Trans. Geosc. Rem. Sens.*, Vol. 47, No. 10, 3031–3038, 2008.
18. Bertero, M. and P. Boccacci, *Introduction to Inverse Problems in Imaging*, Institute of Physics, Bristol, UK, 1998.
19. Liseno, A., F. Soldovieri, and R. Pierri, "Improving a shape reconstruction algorithm with thresholds and multi-view data," *AEU, Int. J. Electron. Commun.*, Vol. 58, 118–124, 2004.
20. Solimene, R. and R. Pierri, "Number of degrees of freedom of the radiated field over multiple bounded domains," *Opt. Lett.*, Vol. 32, No. 21, 3113–3115, 2007.
21. Brancaccio, A., G. Leone, and R. Pierri, "Information content of Born scattered fields: Results in the circular cylindrical case," *Journal of the Optical Society of America A*, Vol. 15, 1909–1917, 1998.
22. Persico, R., F. Soldovieri, and G. Leone, "A microwave tomographic imaging approach for multibistatic configuration: The choice of the frequency step," *IEEE Trans. Instrum. Meas.*, Vol. 55, 1926–1934, 2006.
23. Dehmollaian, M., M. Thiel, and K. Sarabandi, "Through-the-wall imaging using differential SAR," *IEEE Trans. Geosc. Rem. Sens.*, Vol. 47, No. 5, 1289–1296, 2009.
24. Debes, C., M. G. Amin, and A. M. Zoubir, "Target detection in single- and multiple- view through-the-wall radar imaging," *IEEE Trans. Geosci. Remote Sens.*, Vol. 47, No. 5, 1349–1361, 2009.
25. Li, J. and E. G. Zelnio, "Target detection with synthetic aperture radar," *IEEE Trans. Aerosp. Electr. Syst.*, Vol. 32, 613–627, 1996.